Tribology Letters (2022) 70:103
https://doi.org/10.1007/s11249-022-01642-y

ORIGINAL PAPER

Quality Control Metrics to Assess MoS_2 Sputtered Films for Tribological Applications

Tomas F. Babuska[1,2,3] · John F. Curry[2] · Michael T. Dugger[2] · Morgan R. Jones[2] · Frank W. DelRio[2] · Ping Lu[2] · Yan Xin[4] · Tomas Grejtak[1,3] · Robert Chrostowski[6,7] · Filippo Mangolini[6,7] · Nicholas C. Strandwitz[5] · Md Istiaque Chowdhury[5] · Gary L. Doll[8] · Brandon A. Krick[1]

Received: 27 April 2022 / Accepted: 6 August 2022 / Published online: 30 August 2022

Abstract
Pure molybdenum disulfide (MoS_2) solid lubricant coatings could attain densities comparable to doped films (and the associated benefits to wear rate and environmental stability) through manipulation of the microstructure via deposition parameters. Unfortunately, pure films can exhibit highly variable microstructures and mechanical properties due to processes that are not controlled during deposition (i.e., batch-to-batch variation). This work focuses on developing a relationship between density, hardness, friction, and wear for pure sputtered MoS_2 coatings. Results show that dense films ($\rho = 4.5$ g/cm^3) exhibit a 100× lower wear rate compared to porous coatings ($\rho = 3.04$–3.55 g/cm^3). The tribological performance of high density pure MoS_2 coatings is shown to surpass that of established composite coatings, achieving a wear rate 2×($k = 5.74 \times 10^{-8}$ mm^3/Nm) lower than composite MoS_2/Sb_2O_3/Au in inert environments.

Keywords MoS_2 · Density · XRD · RBS · TEM · Hardness · Nanoindentation

1 Introduction

Molybdenum disulfide (MoS_2) solid lubricants have historically been used as coatings in space applications because of their low friction coefficients ($\mu < 0.05$) and wear rates ($k < 1 \times 10^{-6}$ mm^3/Nm) in inert and vacuum environments [1–3]. Pure MoS_2 coatings are not commonly used in terrestrial applications due to high wear rates and oxidation when exposed to water and oxygen [4–11]. To mitigate adverse interactions in terrestrial environments, dopants such as C, Sb_2O_3, Au, Ni, Ta, and Ti are commonly added to improve the tribological performance and environmental robustness [12–20]. While reported mechanisms for performance improvement of composite coatings vary depending on additives, composites such as MoS_2/Sb_2O_3/Au have been shown to help facilitate the expression and retention of MoS_2 at the interface through agglomeration of Au nanoparticles [21]. Other composites such as $MoS_2/C/Sb_2O_3$ have been shown to exhibit extremely low shear strengths. The sliding interface of $MoS_2/C/Sb_2O_3$ changes during sliding depending on the environment, with the surface becoming carbon-rich in humid testing conditions and MoS_2-rich in dry, inert environments [22].

A common hypothesis for the improved environmental resilience of composite MoS_2 coatings involves densification and hardening imparted by dopants [23–28]. Sputtered pure MoS_2 coatings have been shown to exhibit low densities ($\rho \sim 3.3$–4 g/cm^3, theoretical = 4.8–5.06 g/cm^3 [29, 30]), which varies depending on coating microstructure

✉ Brandon A. Krick
bkrick@fsu.edu

1 FAMU-FSU College of Engineering, Florida State University, Tallahassee, USA

2 Material, Physical and Chemical Sciences Center, Sandia National Laboratories, Albuquerque, USA

3 Mechanical Engineering Department, Lehigh University, Bethlehem, USA

4 National High Magnetic Field Laboratory, Florida State University, Tallahassee, USA

5 Materials Science and Engineering Department, Lehigh University, Bethlehem, USA

6 Walker Department of Mechanical Engineering, The University of Texas at Austin, Austin, USA

7 Texas Materials Institute, The University of Texas at Austin, Austin, USA

8 College of Engineering and Polymer Science, The University of Akron, Akron, USA

[31]. Buck [31] observed the density of sputter-deposited amorphous coatings ($\rho \sim 3.3$ g/cm^3) was lower than that of crystalline coatings ($\rho \sim 3.95$ g/cm^3 for basally oriented coatings) due to the presence of microscopic vacancies and a high degree of disorder. Lince et al. [32] found that a higher oxygen content in $MoS_{2-x}O_x$ coatings led to an increase in film density due to a reduction in crystallite size. Interactions between oxygen molecules and MoS_2 increased the defect density of the coating, thereby forming a disordered microstructure [32]. Techniques such as ion-beam assisted deposition (IBAD) have been shown to improve both the density of pure MoS_2 coatings ($\rho \sim 4.4$ g/cm^3) and wear resistance in humid and dry environments [29].

A prevailing hypothesis for enhanced wear resistance of doped-MoS_2 is that it is linked to improved coating density [23–28], though there is little to no direct evidence or a well-developed fundamental understanding of the role of this relationship present in the literature. A major barrier to this understanding lies in the difficulty in depositing fully dense pure films, or even films with consistent density. Variability in coating morphology is one of the main challenges limiting the widespread commercial use of sputtered pure MoS_2 films in engineering applications.

From a *research* perspective, understanding temperature dependence, environmental resilience, or load-dependent friction behavior becomes even more challenging when coating microstructure varies from one deposition to the next. Relationships between detailed coating structure and deposition parameters such as substrate temperature [33, 34], argon partial pressure [31, 32], bias voltage [37], and target-substrate distance [8] have been studied for decades. While many parameters are controllable during deposition, there exist other variables and/or by-products that cannot. For instance, Buck [38] studied the effects of water vapor in the plasma on the microstructure and tribological behavior of MoS_2 coatings. By varying the partial pressure of water, he showed that increased water vapor produced low density, less crystalline coatings that exhibited poor wear resistance. A secondary source of water vapor was also found to be a result of substrate heating during deposition via desorption of water from surfaces. The study found this source of contamination also led to less wear resistant coatings. Interestingly, substrate heating is often changed to improve the performance of MoS_2 coatings, yet it can have a negative effect depending on the cleanliness of the system.

From an *applied* perspective, sputtered MoS_2 films are a preferred solid lubricant coating in inert environments, such as vacuum and space applications. However, despite the best efforts by coatings developers, batch-to-batch variations in film properties, which originate from difficulties in precisely controlling mutually influencing deposition parameters, pose significant challenges for hardware engineers owing to the resulting variability in functional behaviors, including tribological performance. Typically, aerospace hardware manufacturers provide witness coupons for each coating batch and subject them to in-house testing designed to qualify the batch. In recent years, several high-performance MoS_2 based composites have fallen out of favor with hardware engineers due to the inability to reliably achieve the same caliber of tribological performance they once did. While the motivation for more wear resistant, lower friction, and environmentally agnostic materials always remains, there is an applied need to develop metrics to quantify what properties make universally "*good*" MoS_2 coatings and encourage an understanding of what variables during or prior to deposition may be at play to disrupt this. This information will be invaluable in ensuring the quality and consistency of MoS_2 films, as well as metrics that can enable future materials discovery and optimization of film composition and structure for a range of applications.

Given that even experienced commercial suppliers of sputtered MoS_2 coatings can produce films with varying structure and performance due to uncontrolled deposition parameters, a method is needed to efficiently inspect coatings for critical attributes that will insure adequate tribological performance in the intended application. The purpose of this work is to show that density and hardness can be used as quality control metrics to insure the tribological performance of pure sputtered MoS_2 coatings.

2 Experimental Methods

2.1 Materials Synthesis

Two manufacturers were asked to provide dense, nanocrystalline, pure MoS_2 coatings in two separate deposition runs. These were requested to understand if (1) comparable coatings (i.e., orientation, porosity, tribological performance) could be made by separate manufacturers and, (2) if the same manufacturer could provide two identical batches of coatings. The samples include a "Low-Density Coating #1" designated here as LD-1, a "Low-Density Coating #2" designated LD-2, and a "High-Density Coating" designated HD-1; sample designations were based on the results of characterization presented later in this manuscript.

2.1.1 Deposition of LD-1

Pure MoS_2 films were deposited in a vacuum deposition system (base pressure 5×10^{-6} torr) equipped with both radio frequency (RF) and direct current (DC) magnetrons. The substrates were affixed to a rotating stage that was biased at 50 VDC. The RF magnetron was used to sputter MoS_2, and the DC magnetron was used to sputter a 99.99% pure titanium (Ti) target. The Ti target was sputtered first to create

a ~ 100 nm thick Ti adhesion layer between the steel substrate followed by a ~ 200 nm gradient layer of Ti/MoS_2 and then a ~ 800 nm thick pure MoS_2 coating. Target powers were kept at 80 and 120 W, respectively.

2.1.2 Deposition of HD-1 and LD-2

Pure MoS_2 coatings (~ 1 μm thick) were deposited on polished 440C steel substrates (~ 20 nm R_a roughness) with a 10 nm Cr adhesion layer (using arc evaporation) via DC magnetron sputtering using 1.5 mTorr Ar and a 3″ MoS_2 target at 150 W and 30 V bias for 30 min. Identical processing conditions were used to produce HD-1 and LD-2.

2.2 Mechanical Test Methods

2.2.1 Hardness Measurements

Hardness values of MoS_2 films were determined via nanoindentation on a Hysitron TI980 equipped with a Berkovich tip. Prior to experimental testing, the tip area function and load frame compliance were calibrated over the entire load range of the instrument with fused silica as the reference material. 5 × 5 indent arrays with a 10 μm spacing between indents were performed on each film. The maximum load in the load function was 1 mN. For each indent, a CMX (continuous measurement of X) load function was used, consisting of a constant strain-rate load superimposed with a 220 Hz oscillating load. The strain rate was kept constant at 0.123 s^{-1} to mitigate strain-rate effects and the oscillating load was employed to provide depth-dependent data. The instantaneous hardness H was calculated by $H = F_{max}/A$, where F_{max} is the maximum load and A is the contact area at each depth. H values were averaged over indentation depths between 40 and 100 nm to calculate the mean for each indent, as the mechanical properties in this regime were relatively constant. The reported value for each MoS_2 film represents the mean and standard deviation from the 25 indents.

2.2.2 Tribological Testing

Tribological testing was performed on all three coatings simultaneously using a custom-built ball-on-flat high-throughput linear reciprocating tribometer in a controlled environmental chamber. A normal force of 1 N was applied to a 3 mm diameter 440C ball (~ 1 GPa Hertzian stress) on each sample by a load head consisting of a normal load cell connected perpendicular to the friction load cell (phidgets 100 g micro-load cell). The load head is then connected to a compliant titanium flexure driven by a stepper motor stage. The samples were mounted to a bidirectional linear reciprocating stage and tested at a sliding speed of 2 mm/s. Experiments were performed in a dry N2 environment (Mbraun Labstar pro, $O_2 < 0.5$ ppm, $H_2O < 0.5$ ppm) and air environments at 0%, 30% and 60% RH (± 2% RH) in a separate humidity-controlled enclosure.

2.3 Focused Ion Beam (FIB)/Transmission Electron Microscopy (TEM)

Cross-sections were prepared for transmission electron microscopy TEM analysis using a focused ion beam (FIB) in a Dualbeam ThermoFisher Helios. A 2 μm thick protective Pt layer was deposited by first the electron beam and then the ion beam to ensure the surface was not damaged by the FIB. The lamella was studied with the TEM at 200 kV (JEOL JEM-ARM200cF, Tokyo, Japan) and images were acquired with a Gatan Ultrascan CCD camera. Scanning TEM (STEM) dark-field and bright-field images were acquired with a probe size of 0.078 nm and the images were processed and analyzed in DigitalMicrograph (Gatan, Pleasaton, CA). TEM of LD-2 cross-sections was performed using an aberration corrected scanning TEM (FEI Titan™ G2 80–200 STEM) operated at 200 kV and high-angle annular dark-field (HAADF) imaging.

2.4 X-ray Diffraction (XRD)

A PANalytical Empyrean diffractometer with a Cu X-ray tube at a wavelength of 1.541 Å was used to take the X-ray diffraction (XRD) measurements. A Bragg–Brentano HD mirror with suitable slits were used to shape the incident beam to maximize irradiation on the sample. The diffracted beam was shaped with a 7.5 mm antiscatter slit and a soller slit and detected with a PIXcel3D-Medipix3 1 × 1 area detector in scanning line 1D mode. Symmetric θ-2θ (gonio) scans were taken with a step size of 0.0066° and counting rate of 25 s/step.

2.5 Rutherford Backscatter Spectroscopy (RBS)

Rutherford backscatter spectroscopy (RBS) was performed by Infinita Laboratories, Saratoga, CA. A beam of 1.9 MeV 4He + was used for RBS with detection at a 165° scattering angle. An average beam current of 5 nA with integrated charge of 2.0 μC was used. Coating densities were calculated from RBS areal densities (atm/cm^2), RBS measured composition, and TEM measured thickness. The spot size of the RBS has a diameter of ~ 10 mm, or ~ 78.5 mm^2 analysis region.

3 Results

3.1 Microstructure

3.1.1 Void Concentration

TEM of the films (Figs. 1a–c) shows the void concentration varying from sample to sample. LD-1 (Fig. 1a) and LD-2 (Fig. 1b) exhibit a high concentration of voids throughout the thickness of the coating while HD-1 appears to have significantly less features that could be interpreted as voids at this magnitude.

3.1.2 Crystallographic Orientation

XRD of the three MoS_2 coatings (Fig. 2a) indicates $P6_3/mmc$ hexagonal crystal structure (PDF 01–077-1716) with different orientations. LD-1 has little-to-no (0002) oriented lamella (basal orientation, *i.e.,* the basal plane of the hexagonal crystal is preferentially parallel to substrate) and shows a peak at 33.2° indicating that the coating consists of (10 $\bar{1}$ 0) oriented lamella (edge-oriented) relative to the substrate (*i.e.,* the edge plane is parallel to the substrate). The XRD spectra for LD-2 show no peak at 33.2° yet has a very broad peak at 13.48° likely due to (0002) oriented lamella relative to the substrate (i.e., parallel to the substrate). HD-1 shows three distinct MoS_2 peaks at 12.7°, 33.2° and 59.5° corresponding to (0002), (10 $\bar{1}$ 0) and (11 $\bar{2}$ 0) suggesting a more random crystallographic orientation compared to the

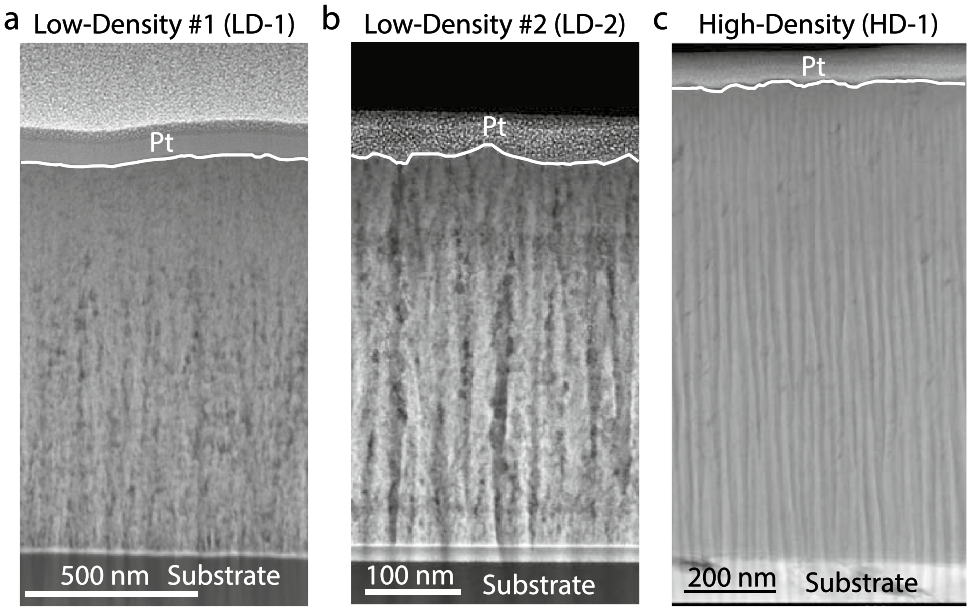

Fig. 1 **A** TEM micrographs of the LD-1 and **B** LD-2 coatings showing high density of voids. **C** TEM micrograph of HD-1 showing little to no voids throughout the coating

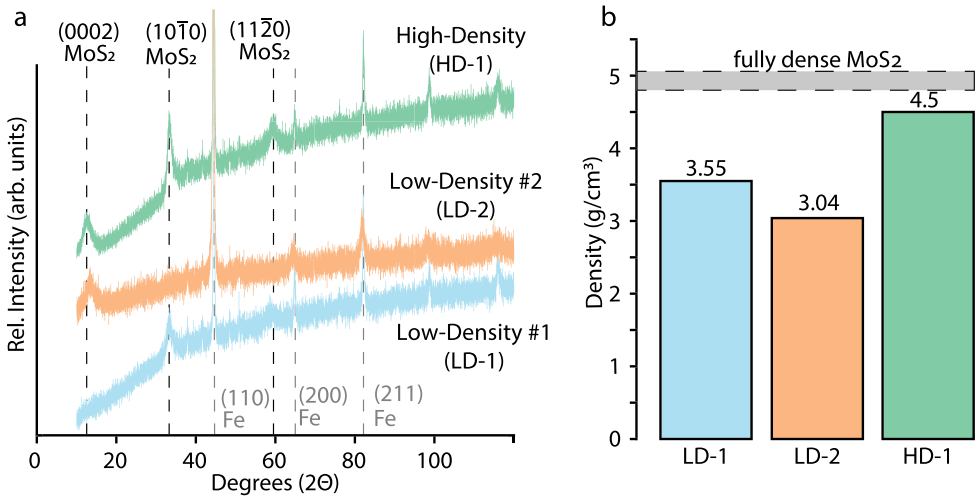

Fig. 2 **A** X-ray diffraction of all three coatings. The HD-1 coating shows peaks for MoS_2 at (002), (100) and (110). The LD-1 coating only has a peak at (100) and LD-2 shows a peak only at (002). **B** Density measurements of all three coatings measured by RBS with reference to fully dense MoS_2 (4.08–5.06 g/cm^3 [29, 30])

preferred orientation in LD-1 and LD-2. HD-1 has higher intensities than LD-1 or LD-2 suggesting that HD-1 is more crystalline.

3.1.3 Film Density and Stoichiometry

Density derived from RBS of all three coatings is shown in Fig. 2b. The LD-1 and LD-2 films are substantially below the density for bulk crystalline MoS_2, while HD-1 has density close to the bulk value of 4.8–5.06 g/cm^3 [29, 30]. Total oxygen content for all three films was measured by RBS to be at or below 5 at%, a value close to the accuracy of the analytical method (±3 at.%). The stoichiometry (S:Mo ratio) of the three coatings was calculated from the aerial densities obtained by RBS. HD-1 is closest to stochiometric with a S:Mo ratio of 1.94, followed by LD-2 (S:Mo = 1.87) and LD-1 (S:Mo = 1.6).

3.2 Mechanical and Tribological Behavior

3.2.1 Hardness and Modulus

Coating hardness for HD-1 was ~ 2–2.75 × greater than that for both LD-1 and LD-2. LD-1 had a measured hardness of 1.6 ± 0.2 GPa while LD-2 had a measured hardness of 2 ± 0.2 GPa. HD-1 exhibited the highest hardness with a value of 4.4 ± 0.6 GPa (shown in Fig. 3 and Table 1). The storage modulus of all three films was measured and had a similar trend with hardness with HD-1 having the highest storage modulus of 83.6 ± 7.2 GPa followed by LD-2 (E = 67.8 ± 4.5 GPa) and LD-1 (E = 50.4 ± 4.1 GPa).

3.2.2 Friction Behavior in Different Environments

The tribological properties of LD-1, LD-2, and HD-1 in environments consisting of air with varying humidity and dry nitrogen are shown in Figs. 4a–e. Measurements in dry N_2 (Fig. 4a) all show MoS_2 behavior consisting of an initially higher cycle one coefficient of friction with a transition (run-in) to lower steady-state coefficient of friction with increased sliding cycles. While the steady-state friction coefficients were nearly identical after 5000 sliding cycles (μ ~ 0.05), the initial friction behavior varied between samples. LD-2 and HD-1 both exhibited lower friction (μ ~ 0.02) for the first 1000 sliding cycles than LD-1 (μ ~ 0.05), and then increased, possibly due to a wear event. The average coefficient of friction for HD-1 was measured in dry N_2 for 250,000 sliding cycles (Fig. 4e) and shows a gradual and minimal increase in the coefficient of friction over the duration of the test from 0.03 to 0.08 and shows no indication of coating failure.

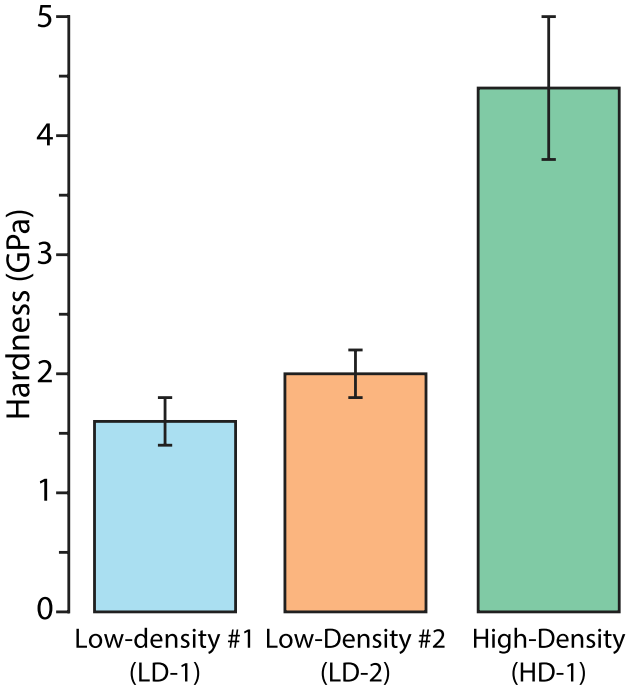

Fig. 3 Average hardness values with corresponding uncertainty intervals for LD-1, LD-2, and HD-1 coatings. Hardness of each specimen was determined from 25 nanoindentation measurements, and the average and standard deviation in the hardness values was calculated for each sample

All three coatings exhibited similarly low friction in dry air with a steady-state coefficient of friction of 0.05 after 2000 sliding cycles (Fig. 4b). LD-2 and HD-1 showed very similar friction behavior for the entire test in dry air and ran-in to low friction after 200 cycles. LD-1 showed prolonged run-in, with a friction coefficient above 0.1 for 600 cycles until it achieved its final steady-state friction coefficient of 0.05.

During tests run in 30% RH air (Fig. 4c) for 200 sliding cycles, LD-1 and HD-1 exhibited friction coefficient between 0.1 and 0.13 while LD-2 exhibited higher friction, μ ~ 0.2, before dropping to 0.08 for the last 60 sliding cycles. In 60% RH air (Fig. 4d), the coefficient of friction over 200 cycles for LD-1 and HD-1 was consistently around 0.1. The coefficient of friction for LD-2 started at 0.1, but after 20 cycles the coefficient of friction increased to 0.25, where it varied sporadically suggesting complete failure of the coating.

3.2.3 Wear Behavior in Different Environments

Wear rates are shown in Fig. 5 and are tabulated in Table 1. HD-1 showed 10–100 × lower wear than the low-density coatings throughout all environments. In dry N_2, HD-1 achieved a wear rate of 5.74×10^{-8} mm^3/Nm while

Table 1 Hardness, storage modulus, density, and wear rates in dry N_2, dry air, 30% RH air and 60% RH air. Note: Cycles to failure with an (*) indicates the maximum cycles coatings were run without failure

Sample	Hardness (GPa)	Storage Modulus (GPa)	Density (g/cm^3)	Wear Rate [mm^3/Nm], (Cycles to Failure)			
				Dry N2	Dry Air	30%RH Air	60% RH Air
Low-Density #1 (LD-1)	1.6 ± 0.2	50.4 ± 4.1	3.55	8.0×10^{-7} $\pm6.5\times10^{-8}$ (50 k*)	5.5×10^{-5} $\pm6.7\times10^{-6}$ (5 k*)	8.6×10^{-5} $\pm7.1\times10^{-6}$ (672)	7.1×10^{-4} $\pm9.7\times10^{-5}$ (100*)
Low-Density #2 (LD-2)	2.0 ± 0.2	67.8 ± 4.5	3.04	1.6×10^{-6} $\pm1.6\times10^{-7}$, (8.6 k)	7.7×10^{-6} $\pm1.2\times10^{-6}$ (2.6 k)	8.3×10^{-5} $\pm4.4\times10^{-6}$ (258)	9.6×10^{-5} $\pm1.3\times10^{-5}$ (100*)
High-Density (HD-1)	4.4 ± 0.6	83.6 ± 7.2	4.5	5.7×10^{-8} $\pm9.9\times10^{-9}$, (250 k*)	1.3×10^{-7} $\pm1.2\times10^{-8}$ (50 k*)	5.1×10^{-6} $\pm5.0\times10^{-7}$ (5 k*)	2.2×10^{-5} $\pm1.4\times10^{-6}$ (1 k*)

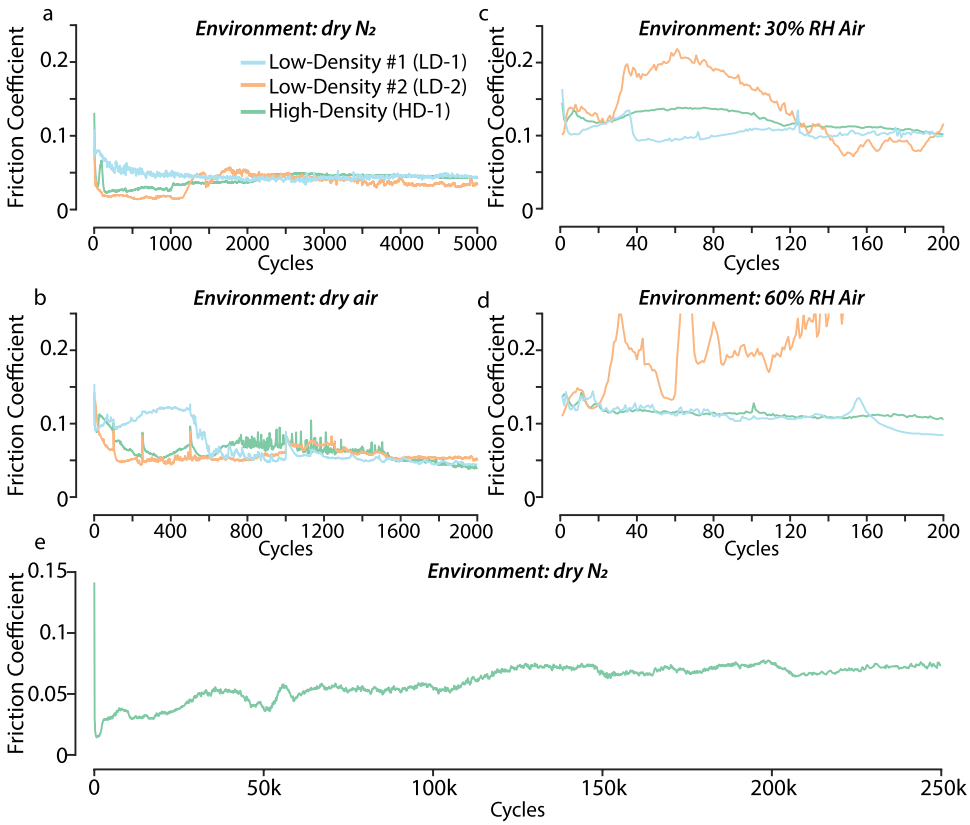

Fig. 4 Friction coefficients of LD-1, LD-2 and HD-1 in dry N_2 (**Aa**), dry air (**B**), 30% RH air (**C**), 60% RH air (**D**) and a 250 k cycles test of HD-1 in dry N_2. **E** The average coefficient of friction for HD-1 in dry N_2 over the entire 250,000 cycle test showing a sustained low coefficient of friction and no indication of failure. Note: Different X-scales

LD-1 had the second lowest wear rate (7.98×10^{-7} mm^3/Nm), followed by LD-2 which had the highest wear rate (1.59×10^{-6} mm^3/Nm). The ultra-low wear rate of HD-1 is further highlighted by the low coefficient of friction sustained for 250,000 sliding cycles (Fig. 4e). In dry air, the wear rates for all three coatings increased, yet HD-1 experienced the smallest change in wear rate with an increase of ~ 2 × (1.28×10^{-7} mm^3/Nm). The wear rate of LD-1 increased in dry air by almost two orders of magnitude (5.47×10^{-5} mm^3/Nm) and LD-2 increased by 7 × in dry air (7.71×10^{-6} mm^3/Nm).

In 30% RH air, the wear rate for HD-1 (5.09×10^{-6} mm^3/Nm) increased by 40 × over its wear rate in dry air, and nearly two orders of magnitude over its wear rate in dry N_2. The measured wear rates for LD-1 and LD-2 were comparable in 30% RH air (8.60×10^{-5} mm^3/Nm and 8.30×10^{-5} mm^3/Nm, respectively), nearly an order of magnitude greater than measurements in dry air.

In 60% RH air, HD-1 had the lowest wear rate of the three coatings tested (2.19×10^{-5} mm^3/Nm) and had a lower wear rate than both LD-1 and LD-2 in 30% RH. The wear rates for the LD-1 and LD-2 were highest in 60% RH air

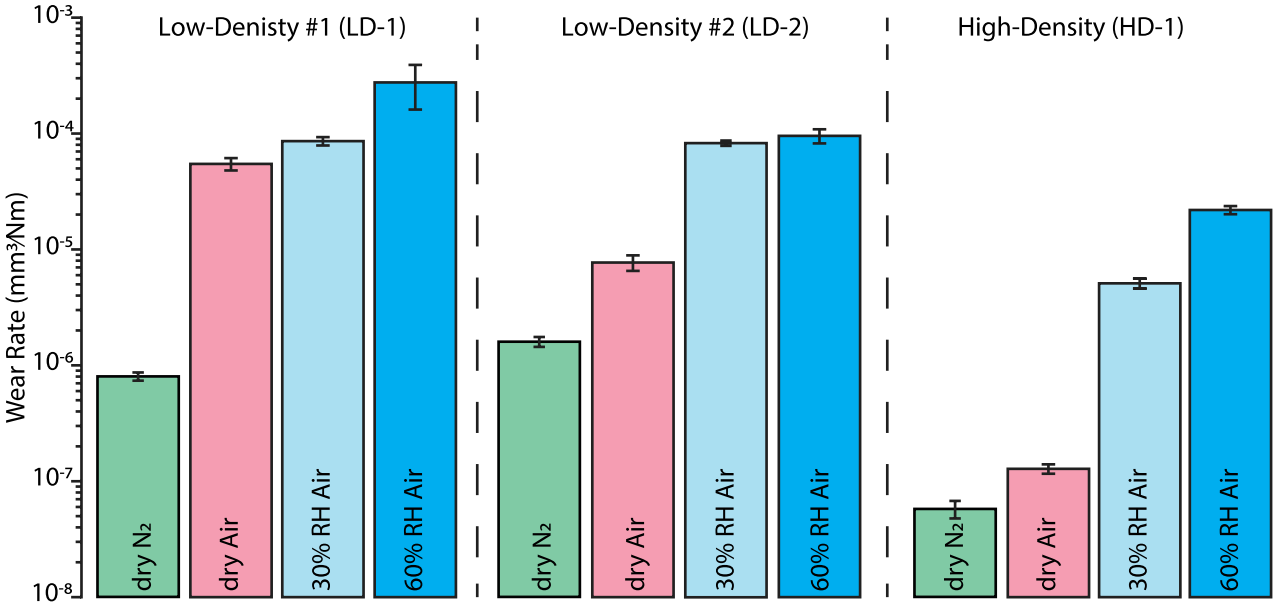

Fig. 5 Wear rate of LD-1, LD-2, and HD-1 in dry N_2, dry air, 30% RH air and 60% RH air. The wear rates are lowest in dry N_2, with HD-1 outperforming LD-1 and LD-2 with 10–100 × lower wear rates in all environments

(7.10×10^{-4} mm^3/Nm and 9.55×10^{-5} mm^3/Nm, respectively), yet the wear rate of LD-2 in 60% RH air was only slightly higher than in 30% RH air. The wear rate of LD-1 in 60% RH air increased by roughly an order of magnitude, more than LD-2.

4 Discussion

Both the LD-2 and HD-1 coatings were manufactured in the same deposition chamber with nominally the same (controllable) deposition parameters, and by the same technician, albeit on different days. Additionally, the LD-1 coating was manufactured in a different chamber but with similar deposition parameters as LD-1 and HD-1. One of the most striking and quantifiable differences between the coating batches is the density. HD-1 ($\rho = 4.5$ g/cm^3) has a density close to that of bulk MoS_2 ($\rho = 4.8$–5.06 g/cm^3), exceeding the average density of IBAD coatings ($\rho = 4.4$ g/cm^3) [29]. Both LD-1 ($\rho = 3.55$ g/cm^3) and LD-2 ($\rho = 3.04$ g/cm^3) have measured density values that are well below HD-1, likely due to the formation of the voids observed in the TEM (Fig. 1).

Differences in density and void formation could be due to variations in crystallite orientation and degree of crystallinity, as indicated by XRD. Buck observed that crystalline pure MoS_2 coatings ($\rho \sim 3.8$–3.95 g/cm^3) are denser than amorphous coatings ($\rho \sim 3.3$ g/cm^3), and that increased basal-orientation improves density due to decreased porosity [31]. Though our results show that LD-1, which is edge-oriented (as indicated by the (10 $\bar{1}$ 0) peak), is denser than the basally oriented LD-2 coating, both coatings have low peak intensities corresponding to their preferential orientations. Orientation and crystallinity can influence the friction and wear behavior of MoS_2, with highly crystalline, basally oriented coatings having lower initial friction coefficients and faster run-in to steady-state friction over amorphous microstructures [39, 40]. Although nanocrystal-amorphous coatings have been reported to have lower wear rates than nanocrystalline coatings [41], in this study it is challenging to decouple the individual effects of orientation and crystallinity from density on the tribological behavior. The impact of orientation on density and void formation is supported by the growth kinetics of MoS_2 during deposition. Low density, porous coatings are a result of the formation of edge-oriented MoS_2 crystallites providing reactive edge-sites for new deposits leading to a high vertical growth rate and decreased horizontal growth rate. As larger, vertically oriented lamellae form, they cause a shadowing effect, blocking incoming deposits resulting in the formation of voids [42, 43]. Void formation can greatly impact hardness. This phenomenon is widely studied in other material systems such as ceramics [44–49] where it has been observed that hardness increases as porosity decreases.

Pure MoS_2 coatings deposited by PVD are typically sub-stoichiometric with a deficiency in sulfur [35, 50] and can have high levels of oxygen in the bulk (> 10%) [32, 51]. Oxygen substituted into the crystal lattice of MoS_2 forms $MoS_{2-x}O_x$ by substituting sulfur and results in a peak shift of the (10 $\bar{1}$ 0) due to a reduced lattice constant [32].

Though the coefficients of friction observed for oxygen rich films are not as low as pure MoS_2 coatings, films containing high amounts of oxygen have been shown to have increased density from a reduced crystallite size, thereby producing lower wear rates than that of pure MoS_2 coatings [32]. Addition of oxygen, which can be viewed as a dopant, means that "pure" is a misnomer for MoS_2 films without dopants because of the added benefits oxygen can impose. In this work, no statistically significant difference in oxygen content in the coatings under investigation was detected. Notably, the oxygen content was very low and close to the accuracy of the analytical tool. While we do not believe that oxygen is contributing to the improved densification of HD-1, it is not unlikely that sources of contamination during the deposition process could introduce unwanted oxygen or water. Sources such as adsorbed water on the deposition chamber walls due to exposure to lab air during sample changing or transfer and a contaminated sputtering target could be key uncontrolled factors that influence the coatings density and tribological behavior.

For MoS_2, relationships between coating porosity, hardness, and wear are not well established. Seynstahl et al. [52] varied the sample substrate rotation during deposition and observed that compact pure MoS_2 coatings with little to no porosity were harder (H = 5.69 GPa) and more wear resistant ($k \sim 1 \times 10^{-7}$ mm^3/Nm) than softer (H ~ 0.06–0.25 GPa), porous films ($k \sim 5 \times 10^{-6}$—2×10^{-5} mm^3/Nm). Although the authors did not directly measure density, we observe a similar trend with HD-1 exhibiting a higher hardness (H = 4.4 GPa) and lower wear rate ($k = 5.74 \times 10^{-8}$ mm^3/Nm) in dry N_2 than both LD-1 (H = 1.6 GPa, $k = 7.98 \times 10^{-7}$ mm^3/Nm) and LD-2 (H = 2 GPa, $k = 1.59 \times 10^{-6}$ mm^3/Nm). While density is a major factor contributing to the increased hardness of HD-1, the discrepancy between hardness and density for LD-1 and LD-2 could be due to differences in coating orientation. Though both LD-1 and LD-2 have weak peak intensities indicating nanocrystalline/amorphous microstructures, there is weak preferential vertical orientation of LD-1 (*i.e.,* basal planes parallel to the indentation axis), compared to the more basally oriented LD-2 (basal planes perpendicular to the indentation axis), allowing for deformation to occur between low shear strength basal planes as the coating is deformed. For vertically oriented coatings, the indenter tip can advance further into the coating by pushing the columns apart resulting in a lower measured hardness [44]. The high hardness and density of HD-1 produced a greater wear resistance than that of widely established composite films such as $MoS_2/Sb_2O_3/Au$ ($k \sim 1 \times 10^{-7}$ mm^3/Nm [21]) in dry N_2 environments. Improvements in the wear rates imparted by density and hardness are also observed in humid environments (Fig. 5), suggesting that wear performance measured in humid air could be a metric for a quality MoS_2 coatings, which for practical flight hardware, could be a useful metric if inert environments are unavailable or impractical to use.

Density as a driving factor for low wear MoS_2 coatings, and hardness as an indicator of coating density, provides a useful metric for the qualification of MoS_2 coatings to be used in practical applications. The low measured hardness of LD-1 and LD-2 would, for instance, indicate to an engineer that the batch of coatings will not meet specifications and should not be used. By using hardness as a metric, timely tribological testing of coating batches or costly characterization techniques such as RBS can be avoided, and only performed on batches such as HD-1 which meet an adequate hardness threshold. Additional useful metrics such as crystallinity and orientation, measured by XRD, would help provide a fast and accurate indication of a quality film.

5 Conclusions

Uncontrolled variation in mechanical properties of sputter deposited pure MoS_2 has limited their use in engineering applications. In this work, relationships between the mechanical properties and density of pure MoS_2 coatings were developed to establish deterministic parameters for high-quality coatings. Three batches of pure MoS_2 coatings were deposited using similar parameters, yet the wear rates of the coatings varied by ~ 100 × in dry N_2. Density of the coatings showed that each coating batch varied in density with the highest density, lowest wear coating ($k = 5.74 \times 10^{-8}$ mm^3/Nm, $\rho = 4.5$ g/cm^3) having little to no void formation and achieving a density close to bulk MoS_2. The other coatings both had low density ($\rho = 3.04$ and 3.55 g/cm^3) and significant void formation throughout the coatings. Nanoindentation showed distinct hardness and modulus differences between dense (H = 4.4 GPa, E = 83.7 GPa) and porous (H = 1.6–2 GPa, E = 50.4–67.8 GPa) coatings, correlating to changes in density and coating orientation. These results suggest that density is one of the dominant factors contributing to low wear rates for MoS_2 coatings and that the hardness of a coating is a key indicator of high-performance coatings. Furthermore, using hardness as a key metric to determine coating batch quality could help in reducing time consuming tribological testing or complex and expensive characterization.

Acknowledgements G.L.D. would like to acknowledge the assistance and contributions of the students and staff of the Timken Engineered Surfaces Laboratory at the University of Akron.

Funding This material is based upon work supported by the National Science Foundation under Grant No. 2027029, 1826251, and NSF GRFP No. 1842163. TEM work was performed at the National High Magnetic Field Laboratory, which is supported by National Science Foundation Cooperative Agreement No. DMR-1644779 and the State

of Florida. G.L.D. was supported by funding from the Center for Surface Engineering and Lubrication Research. F.W.D. was supported by the Center for Integrated Nanotechnologies, a Department of Energy office of Basic Energy Sciences user facility. This work was funded by the Laboratory Directed Research and Development (LDRD) program at Sandia National Laboratories, a multi-mission laboratory managed and operated by National Technology and Engineering Solutions of Sandia, LLC., a wholly owned subsidiary of Honeywell International, Inc., for the U.S. Department of Energy's National Nuclear Security Administration under contract DE-NA0003525. This paper describes objective technical results and analysis. Any subjective views or opinions that might be expressed in the paper do not necessarily represent the views of the U.S. Department of Energy or the United States Government.

Declarations

Competing interest The authors have no competing interests to disclose.

References

1. Donnet, C., Martin, J.M., le Mogne, T., Belin, M.: Super-low friction of MoS_2 coatings in various environments. Tribol. Int. **29**(2), 123–128 (1996)
2. Hilton, M.R., Fleischauer, P.D.: Applications of solid lubricant films in spacecraft. Surf. Coat. Technol. **54–55**, 435–441 (1992)
3. Roberts, E.W.: Ultralow friction films of MoS_2 for space applications. Thin Solid Films **181**(1–2), 461–473 (1989)
4. Pritchard, C., Midgley, J.W.: The effect of humidity on the friction and life of unbonded molybdenum disulphide films. Wear **13**(1), 39–50 (1969)
5. Serpini, E., Rota, A., Ballestrazzi, A., Marchetto, D., Gualtieri, E., Valeri, S.: The role of humidity and oxygen on MoS_2 thin films deposited by RF PVD magnetron sputtering. Surf. Coat. Technol. **319**, 345–352 (2017)
6. Panitz, J.K.G., Pope, L.E., Lyons, J.E., Staley, D.J.: Tribological properties of MoS_2 Coatings in vacuum, low relative humidity and high relative humidity environments. J. Vacuum Sci. Technol. A **6**(3), 1166 (1987)
7. Zhao, X., Zhang, G., Wang, L., Xue, Q.: The tribological mechanism of MoS_2 film under different humidity. Tribol. Lett. **65**(2), 1 (2017)
8. Vierneusel, B., Schneider, T., Tremmel, S., Wartzack, S., Gradt, T.: Humidity resistant MoS_2 coatings deposited by unbalanced magnetron sputtering. Surf. Coat. Technol. **235**, 97–107 (2013)
9. Fleischauer, P.D.: Effects of crystallite orientation on environmental stability and lubrication properties of sputtered moS. ASLE Trans. **27**(1), 82–88 (1984)
10. Zhao, X., Perry, S.S.: The role of water in modifying friction within MoS_2 sliding interfaces. ACS Appl. Mater. Interfaces **2**(5), 1444–1448 (2010)
11. Khare, H.S., Burris, D.L.: Surface and subsurface contributions of oxidation and moisture to room temperature friction of molybdenum disulfide. Tribol. Lett. **53**(1), 329–336 (2014)
12. Scharf, T.W., Goeke, R.S., Kotula, P.G., Prasad, S.V.: Synthesis of Au-MoS_2 nanocomposites: thermal and friction-induced changes to the structure. ACS Appl. Mater. Interfaces **5**(22), 11762–11767 (2013)
13. Lince, J.R.: Tribology of co-sputtered nanocomposite Au/MoS_2 solid lubricant films over a wide contact stress range. Tribol. Lett. **17**(3), 419–428 (2004)
14. Lince, J.R., Kim, H.I., Adams, P.M., Dickrell, D.J., Dugger, M.T.: Nanostructural, electrical, and tribological properties of composite Au-MoS_2 coatings. Thin Solid Films **517**(18), 5516–5522 (2009)
15. Wahl, K.J., Seitzman, L.E., Bolster, R.N., Singer, I.L.: Low-friction, high-endurance, ion-beam-deposited Pb-Mo-S coatings. Surf. Coat. Technol. **73**(3), 152–159 (1995)
16. Wahl, K.J., Dunn, D.N., Singer, I.L.: Wear behavior of Pb-Mo-S solid lubricating coatings. Wear **230**(2), 175–183 (1999)
17. Centers, P.W.: Tribological performance of MoS2 compacts containing MoO_3, Sb_2O_3 or MoO_3 and Sb_2O_3. Wear **122**(1), 97–102 (1988)
18. Wang, X., Xing, Y., Ma, S., Zhang, X., Xu, K., Teer, D.G.: Microstructure and mechanical properties of MoS_2/titanium composite coatings with different titanium content. Surf. Coat. Technol. **201**(9–11), 5290–5293 (2007)
19. Renevier, N.M., Fox, V.C., Teer, D.G., Hampshire, J.: Coating characteristics and tribological properties of sputter-deposited MoS2/metal composite coatings deposited by closed field unbalanced magnetron sputter ion plating. Surf. Coat. Technol. **127**(1), 24–37 (2000)
20. Serles, P., et al.: High performance space lubrication of MoS_2 with tantalum. Adv. Func. Mater. **32**(20), 1 (2022)
21. Scharf, T.W., Kotula, P.G., Prasad, S.V.: Friction and wear mechanisms in MoS_2/Sb_2O_3/Au nanocomposite coatings. Acta Mater. **58**(12), 4100–4109 (2010)
22. Muratore, C., Voevodin, A.A.: Chameleon Coatings: Adaptive Surfaces to Reduce Friction and Wear in Extreme Environments, 2009
23. Renevier, N.M., Lobiondo, N., Fox, V.C., Teer, D.G., Hampshire, J.: Performance of MoS_2/metal composite coatings used for dry machining and other industrial applications. Surf. Coat. Technol. **123**(1), 84–91 (2000)
24. Ding, X.Z., Zeng, X.T., He, X.Y., Chen, Z.: Tribological properties of Cr- and Ti-doped MoS_2 composite coatings under different humidity atmosphere. Surf. Coat. Technol. **205**(1), 224–231 (2010)
25. Gu, L., Ke, P., Zou, Y., Li, X., Wang, A.: Amorphous self-lubricant MoS_2-C sputtered coating with high hardness. Appl. Surf. Sci. **331**, 66–71 (2015)
26. Cai, S., et al.: Friction and wear mechanism of MoS_2/C composite coatings under atmospheric environment. Tribol. Lett. **65**, 1 (2017)
27. Lincea, J.R., Hilton, M.R., Bommannavar, A.S.: Metal incorporation in sputter-deposited MoS_2 films studied by extended x-ray absorption fine structure. J. Mater. Res. **10**(8), 2091–2105 (1995)
28. Simmonds, M.C., Savan, A., Pflüger, E., van Swygenhoven, H.: Mechanical and tribological performance of MoS_2 co-sputtered composites. Surf. Coat. Technol. **126**(1), 15–24 (2000)
29. Bolster, R.N., Singer, I.L., Wegand, J.C., Fayeulle, S., Gossett, C.R.: Preparation by ion-beam-assisted deposition, analysis and

tribological behavior of MoS_2 films. Surf. Coat. Technol. **46**(2), 207–216 (1991)
30. Haynes, W.M.: CRC Handbook of Chemistry and Physics, 92nd edn. CRC Press, Boca Raton, FL (2011)
31. Buck, V.: Structure and density of sputtered MoS_2-films. Vacuum **36**(1–3), 89–94 (1986)
32. Lince, J.R., Hilton, M.R., Bommannavar, A.S.: EXAFS of sputter-deposited MoS_2 films. Thin Solid Films **264**(1), 120–134 (1995)
33. Lince, J.R., Fleischauer, P.D.: Crystallinity of rf-sputtered MoS_2 films. J. Mater. Res. **2**(6), 827–838 (1987)
34. Spalvins, T.: Tribological properties of sputtered MoS_2 films in relation to film morphology. Thin Solid Films **73**(2), 291–297 (1980)
35. Dimigen, H., Hübsch, H., Willich, P., Reichelt, K.: Stoichiometry and friction properties of sputtered MoS_x layers. Thin Solid Films **129**(1–2), 79–91 (1985)
36. Moser, J., Lèvy, F.: MoS_{2-x} lubricating films: structure and wear mechanisms investigated by cross-sectional transmission electron microscopy. Thin Solid Films **228**(1–2), 257–260 (1993)
37. Panitz, J.K.G., Pope, L.E., Hills, C.R., Lyons, J.E., Staley, D.J.: A statistical study of the combined effects of substrate temperature, bias, annealing and a Cr_3Si_2 undercoating on the tribological properties of r.f. sputtered MoS_2 coatings. Thin Solid Films **154**(1–2), 323–332 (1987)
38. Buck, V.: Preparation and properties of different types of sputtered MoS_2 films. Wear **114**(3), 263–274 (1987)
39. Curry, J.F., et al.: Highly oriented MoS_2 coatings: tribology and environmental stability. Tribol. Lett. **64**(1), 1–9 (2016)
40. Curry, J.F., et al.: Impact of microstructure on MoS_2 oxidation and friction. ACS Appl. Mater. Interfaces. **9**(33), 28019–28026 (2017)
41. Serles, P., et al.: Structure-Dependent Wear and Shear Mechanics of Nanostructured MoS_2 Coatings. Adv. Mater. Interfaces **7**(14), 1901870 (2020)
42. Moser, J., Liao, H., Levy, F.: Rapid Communication: Texture characterization of sputtered MoS_2 thin films by cross-sectional TEM analysis. J. Phys. D Appl. Phys. **23**(5), 624–626 (1990)
43. P. A. Bertrand, Orientation of rf-sputter-deposited MoS_2 films
44. Jang, B.K., Matsubara, H.: Influence of porosity on hardness and Young's modulus of nanoporous EB-PVD TBCs by nanoindentation. Mater. Lett. **59**(27), 3462–3466 (2005)
45. Paneto, F.J., et al.: Effect of porosity on hardness of Al_2O_3–$Y_3Al_5O_{12}$ ceramic composite. Int. J. Refract Metal Hard Mater. **48**, 365–368 (2015)
46. Luo, J., Stevens, R.: Porosity-dependence of elastic moduli and hardness of 3Y-TZP ceramics. Ceram. Int. **25**(3), 281–286 (1999)
47. Milman, Y.V., Chugunova, S.I., Goncharova, I.V., Chudoba, T., Lojkowski, W., Gooch, W.: Temperature dependence of hardness in silicon-carbide ceramics with different porosity. Int. J. Refract. Met. Hard Mater. **17**, 361–368 (1999)
48. Soroka, I.: Interrelation of Hardness, Modulus of Elasticity, and Porosity in Various Gypsum Systems. J. Am. Ceram. Soc. **51**, 337–340 (1968)
49. Hoepfner, T.P., Case, E.D.: The influence of the microstructure on the hardness of sintered hydroxyapatite. Ceram. Int. **29**(6), 699–706 (2003)
50. Weiss, V., et al.: Reactive magnetron sputtering of molybdenum sulfide thin films: in situ synchrotron x-ray diffraction and transmission electron microscopy study. J. Appl. Phys. **95**(12), 7665–7673 (2004)
51. Lince, J.R.: MoS2-xOx solid solutions in thin films produced by rf- sputter- deposition. J. Mater. Res. **5**(1), 218–222 (1990). https://doi.org/10.1557/JMR.1990.0218
52. Seynstahl, A., Krauß, S., Bitzek, E., Meyer, B., Merle, B., Tremmel, S.: Coatings Microstructure, Mechanical Properties and Tribological Behavior of Magnetron-Sputtered MoS_2 Solid Lubricant Coatings Deposited under Industrial Conditions, 2021